Colloids and Surfaces B: Biointerfaces 228 (2023) 113422

Contents lists available at ScienceDirect

Colloids and Surfaces B: Biointerfaces

journal homepage: www.elsevier.com/locate/colsurfb

Properties and cellular uptake of photo-triggered mixed metallosurfactant vesicles intended for controlled CO delivery in gas therapy

Jan Trallero [a], Mercedes Camacho [b], Maribel Marín-García [a], Elena Álvarez-Marimon [a], Núria Benseny-Cases [a,c,*], Ramon Barnadas-Rodríguez [a,**]

[a] Universitat Autònoma de Barcelona, Biophysics Unit/Center for Biophysical Studies, Department of Biochemistry and Molecular Biology, Faculty of Medicine, 08193 Cerdanyola del Vallès, Spain
[b] Institut de Recerca de l'Hospital de la Santa Creu i Sant Pau - Centre CERCA, Genomics of Complex Diseases, Barcelona, Spain
[c] Consorcio para la Construcción Equipamiento y Explotacion del Laboratorio de Luz Sincrotron, ALBA Synchrotron Light Source, 08290 Cerdanyola del Vallès, Catalonia, Spain

ARTICLE INFO

Keywords:
Cell internalization
Colloid
CORM
Liposome
Metallosome
Self-assembly

ABSTRACT

The scientific relevance of carbon monoxide has increased since it was discovered that it is a gasotransmitter involved in several biological processes. This fact stimulated research to find a secure and targeted delivery and lead to the synthesis of CO-releasing molecules. In this paper we present a vesicular CO delivery system triggered by light composed of a synthetized metallosurfactant (TCOL10) with two long carbon chains and a molybdenum-carbonyl complex. We studied the characteristics of mixed TCOL10/phosphatidylcholine metallosomes of different sizes. Vesicles from 80 to 800 nm in diameter are mainly unilamellar, do not disaggregate upon dilution, in the dark are physically and chemically stable at 4 °C for at least one month, and exhibit a lag phase of about 4 days before they show a spontaneous CO release at 37 °C. Internalization of metallosomes by cells was studied as function of the incubation time, and vesicle concentration and size. Results show that large vesicles are more efficiently internalized than the smaller ones in terms of the percentage of cells that show TCOL10 and the amount of drug that they take up. On balance, TCOL10 metallosomes constitute a promising and viable approach for efficient delivery of CO to biological systems.

1. Introduction

The discovery in the mid-20th century that poisonous CO is endogenously produced in our bodies leading to other surprising knowledge sometime later: is not just a degradation product that has to be eliminated, but also a necessary gasotransmitter (such as NO and H_2S) that regulates diverse biological processes [1]. This condition opened the door for searching for biomedical applications of the gas by means of controlled exogenous delivery, but this goal included a necessary challenge that is very difficult to solve: its administration. The most direct route is inhalation, which can be used only if an extremely accurate control is carried out both on the dose and on the subject, whose carboxyhemoglobin level in the blood must be continuously monitored during the administration. These mandatory restraints, along with the systemic and non-specific diffusion of the gas involved in inhalation, enhanced the search for alternative methods. Thus, most current research in this field is focused on around the design of safe, efficient and selective CO delivery systems. In turn, day-to-day scientific works have allowed the discovery of new gas applications. It is known, for example, that it has effect on cardiovascular alterations, stem cell regulation, nociception, cancer processes, microbial growth, inflammation diseases, and that facilitates organ transplantation, etc. [2–5].

There are alternative delivery strategies to inhalation, in which the gas is directly transported or contained by different types of delivery systems. This is the case for aqueous CO-saturated solutions that are administered as enemas [6], and lipidic shell structures that contain the gas and release it under ultrasound irradiation [7]. In a similar approach, a hemoglobin derivative is used as a CO carrier because of its high affinity for the gas, and after administration, CO is slowly released [8]. However, most efforts have focused on in the so-called CO-releasing

* Corresponding author at: Universitat Autònoma de Barcelona, Biophysics Unit/Center for Biophysical Studies, Department of Biochemistry and Molecular Biology, Faculty of Medicine, 08193 Cerdanyola del Vallès, Spain.
** Corresponding author.
E-mail addresses: nuria.benseny@uab.cat (N. Benseny-Cases), ramon.barnadas@uab.cat (R. Barnadas-Rodríguez).

https://doi.org/10.1016/j.colsurfb.2023.113422
Received 26 May 2023; Received in revised form 13 June 2023; Accepted 19 June 2023
Available online 21 June 2023
0927-7765/© 2023 The Author(s). Published by Elsevier B.V. This is an open access article under the CC BY-NC-ND license (http://creativecommons.org/licenses/by-nc-nd/4.0/).

molecules (CORMs), chemical structures that bear bonded CO (one or several groups) or precursors. In these cases, CO release can be triggered by several factors such as pH, light (then known as photo-CORM), proteins, temperature, solvents, etc [9–11]. From a structural point of view, there are several families of CORMs, one of which is that composed of metal-carbonyl complexes. These molecules bear CO linked to a transition-metal atom and depending on their water solubility, can be administrated in the bulk or included in other structures/systems (for example, they can be encapsulated into liposomes [12], included in oral tablets that also contain a chemical trigger [13], or entrapped in block copolymer micelles [14]). In all these examples the CORMs maintain their properties and are part of the cargo of a system that protects them from environmental conditions until the CO is released.

There is another approach, in which the metal CORM is a constitutive part of a delivery colloidal system. This is possible because of the properties of metallosurfactants, that is, molecules with hydrophilic and hydrophobic domains that contain one or more metal atoms in their molecular structure. In aqueous media most of these molecules, with or without the participation of lipids such as phospholipids and/or cholesterol, form vesicles, known as metallosomes [15–18]. If the metallosurfactant contains a transition metal bonded to some CO ligands, either in the hydrophilic or in the hydrophobic domain, then a metallosome with CO releasing properties can be obtained [19,20].

The present work focuses on mixed metallosomes composed of phosphatidylcholine and a photo-CORM metallosurfactant (TCOL10) sensitive to 365 nm and visible light which triggers the CO release by breaking the coordinate CO-Mo bond [21,22]. The hydrophobic domain of TCOL10 contains a molybdenum carbonyl complex with four CO groups and two hydrocarbon chains of ten carbon atoms; at the end of each chain there is a negatively charged sulfonate group and both are the polar head of the molecule (SupplMat-1). TCOL10 spontaneously forms pure metallosomes in water, which disaggregate when diluted, making them unsuitable for biomedical applications. When mixed with phosphatidylcholine at any molar ratio metallosomes are formed, however they are very large vesicles, and size reduction is mandatory for their use in biological systems. However, the stability of smaller vesicles could be jeopardized because of the very different molecular shapes of the two components, which makes efficient bilayer packing difficult, particularly for particles with a small radius. Therefore, the use of mixed TCOL10/phospholipid metallosomes as CO delivery systems presents several challenges. For example; to what extent is it possible to obtain small vesicles and what are their characteristics? Are they stable upon dilution and undergo physical and/or chemical degradation? Do they interact with cells? If so, is it possible to describe cellular uptake as function of vesicle size, concentration, and time of incubation? Are TCOL10 mixed metallosomes a viable system for CO release to cells? These and some other important related questions about this particular system constituted by a metallosurfactant were the starting point of the work we present here, and they are answered below.

2. Materials and methods

2.1. Lipids, reagents and solvents

Soybean phosphatidylcholine (SPC; 97%; MW 775 Da) was obtained from Avanti Polar Lipids. The metallosurfactant with CO releasing properties was obtained according to the synthesis described by Parera et al.[21] Briefly, the ligand with the structure $Ph_2P(CH_2)_{10}SO_3Na$ substitutes piperidine (pip) in the complex cis-$[Mo(CO)_4(pip)_2]$ and the reaction leads to a complex that bears four CO groups that are prone to be released as CO gas, for example, under light irradiation [23]. This molecule (TCOL10) is a metallosurfactant composed of a hydrophobic domain (the Mo complex and the two hydrocarbon chains) and two polar headgrups (sulfonates) located at the end of these chains. The headgroups confer two negative charges to the molecule at physiological pH (in fact, over a wide pH range).

All reagents used were of analytical grade. Dulbecco's Modified Eagle Medium (DMEM), fetal bovine serum (FBS) and supplement used in cell cultures were obtained from Biological Industries Israel Beit Haemek LTD.

2.2. Vesicle preparation

To obtain SPC liposomes the necessary amount of SPC stock solution in $CHCl_3$ / methanol 1/1 v/v was added to a glass tube and rotovaporated. Once a thin and dry lipidic film was achieved the tub was kept under vacuum overnight, protected from light. Next, large and multilamellar liposomes (with no size control) were obtained by the addition of an aqueous medium to the film and subsequent vortexing. Large metallosomes (liposomes that contain metal atoms in their structure) were obtained in the same way but the required amounts of SPC and TCOL10 organic stock solutions were mixed in a glass tube to produce a 1:3 TCOL10/SPC molar ratio. The volume of aqueous medium added to the dry lipidic films was adjusted to obtain a final TCOL10 concentration of 1 mM (and therefore 3 mM of SPC) in the case of the metallosome suspension and 3 mM for the liposome suspension. The aqueous medium used was DMEM when the suspensions were prepared to perform cell assays since this is the cell incubation medium. However, in the vesicle stability studies PBS was used to avoid any interference from the DMEM components in the infrared analysis. As regards the size of the vesicles, it was regulated by progressive extrusion of the large vesicles obtained by vortex using polycarbonate membranes of the given pores. Extrusions through 800 (six times), 400 (six times) and 200 nm (two times) membrane pores were carried out with a stainless screen holder (Swinny 13 mm) using a syringe, while those through 100 (nine times) and 50 nm (eleven times) were carried out using a Liposofast LF-50 device.

2.3. Vesicle characterization

The size of the vesicles was measured using a dynamic light scattering (DLS) device (Malvern Nano ZS) and the results were expressed as the diameter of the peaks shown in the volume size distribution, their corresponding width (range that encloses 68% of the peak) and polydispersity index. Because the nominal upper range of the analysis by the DLS device is approximately 6 μm, optical microscopy was carried out to verify the existence of vesicles out of this range [24]. To this end, an aliquot of each suspension was placed on a microscope glass slide and several pictures were taken with an Olympus BX50 microscope. A calibration slide was used as reference size for the pictures. After equilibrating their density using Photoshop CS5, the pictures were analyzed using ImageJ to obtain the number distribution of the visible vesicles.

Cryo-Transmission electron microscopy (cryo-TEM) was used to characterize the morphology of the vesicles. It was carried out with a Jeol JEM-2011 microscope at the Microscope Service of the Autonomous University of Barcelona (UAB).

2.4. Chemical stability of the metallosomes

The chemical stability of the metallosurfactant that forms the metallosomes was determined using Fast Fourier infrared spectrometry (FTIR). This technique allows visualization of the relative amount of CO groups in TCOL10 to that of SPC through the corresponding absorption band ratios, which are located at approximately 2020 cm^{-1} and 1735 cm^{-1} respectively. The different location of the absorption peaks of both carbonyls is due to the nature of the bonds between C and O in TCOL10 and SPC. The bond order of the CO group in TCOL10 is higher than in SPC; in TCOL10 it can formally be considered a triple bond while in SPC the CO group is constituted by a double bond. It is known that the infrared CO band of TCOL10 decreases upon irradiation of the metallosomes owing to the release of CO gas, and the monitoring of the previously stated intensity ratio is a rapid method for determining the state of the metallosurfactant [25]. Thus, the stability of 800, 200 and 50 nm

extruded metallosomes was determined in the dark at 37 ºC and 4 ºC for 30 days. At certain time intervals aliquots of the samples were frozen (−80 °C) until analysis. Once unfrozen, each collected sample was placed on CaF_2 infrared windows that were placed in a desiccator protected from light and the water was removed under high vacuum. The obtained dry films were analyzed using an Evariant Cary 660 FTIR spectrometer at the Laboratory of Luminescence and spectroscopy of Biomolecules at the UAB.

2.5. Cell cultures

The toxicity of the suspensions was tested in human dermal fibroblasts using the XTT assay. The cells were seeded in 96 wells culture plates at a density of 7.5×10^3 cells per well and cultured in DMEM containing 10% SBF. After 24 h cells were maintained in DMEM 1% SBF for 24 h before incubation with increasing concentrations of metallosomes (and liposomes) diluted in cell culture medium (DMEM with 1% SBF) for 24 h. After this period, the medium was removed, the cells were rinsed twice with PBS (0.1 mL) and toxicity was assessed using the XTT assay according to the manufacturer's protocol.

The cell internalization assay of metallosomes as function of their size, concentration and incubation time was carried out using human fibroblasts cultured on infrared CaF_2 window (diameter: 2.5 cm, width: 0.5 mm; Crystran Ltd, UK) at 70% confluence, as previously described.[25] Briefly, after 24 h of seeding the cells on the CaF_2 windows placed in 24 well plates, the different treatments were carried out. After the incubation time the cells were washed three times with PBS, fixed for 30 min in 4% paraformaldehyde, and quickly rinsed with deionized water. The culture plates also included one well as a control group (non-treated cells) and two wells with cells that were incubated with 3 mM SPC liposomes of 50 and 800 nm.

2.6. FTIR microscopy internalization assay using synchrotron radiation

The main objective of the present work was to characterize the cell internalization of metallosomes by evaluating three factors: the size of the metallosomes (extruded from 800 to 50 nm); their concentration (from 50 to 1000 μM of TCOL10) and the incubation time (from 2 to 26 h). We carried out an optimized multifactorial experimental design [26]. The levels of the factor combinations were established to fit a centred star and cube design, and to achieve more accuracy an additional external centred cube was included at the extreme values of the factors. The selected absolute values of the factors are shown in Table 1, but to fit them with the selected experimental design a change of variable was done by means of the common logarithm. In this way similar increments are obtained, and the level combinations of the metallosome incubations are close to the centred star and cube design (SupplMat-2). The 23 factor combinations used for the different cell incubations are shown in SupplMat-3.

The windows with fixed cells were analysed by FTIR microscopy using synchrotron light at the MIRAS Beamline of the ALBA synchrotron equipped with a Hyperion 3000 microscope coupled with a Vertex 80 infrared spectrometer (Bruker). The infrared spectra of each sample were obtained with an optical window of 10×10 μm and a resolution of 4 cm^{-1}. A total of 256 or 512 scans were accumulated for each analysed cell, depending on the observed noise. A mean of 37 spectra for any incubation condition were obtained. After the acquisition and prior to the analysis, the spectra showing strong Mie scattering or a low signal-to-noise ratio were rejected. Subsequently, baseline correction was performed and the spectra were normalized by the intensity of CO band of the SPC.

Infrared spectra of a cells show the amide I peak (1680 cm^{-1}) which corresponds to cellular proteins, and if this cell has internalized metallosomes the peak of the characteristic carbonyl groups of TCOL10 (2020 cm^{-1}) should be detected. Thus, on the one hand, the collected spectra allow to know the percentage of cells that presented TCOL10 for each one of the 23 incubation conditions with the metallosomes. And, on the other hand, the relative amount of TCOL10 in the cells can be obtained by the ratio between the absorbance of the CO band of the TCOL10 and that of the amide I band, which is representative of the cellular protein. This ratio was calculated for those spectra that showed the existence of the CO band, and was equaled to 0 in the other cases. The percentage of cells with TCOL10 and the TCOL10 to protein ratio were the responses of the studied factors, and a full polynomial second-order model (Eq. 1) was fitted to them:

$$\text{Response} = k + \alpha_1 \cdot D^* + \alpha_2 \cdot D^{*\,2} + b_1 \cdot C^* + b_2 \cdot C^{*\,2} + c_1 \cdot T^* + c_2 \cdot T^{*\,2} + d_1 \cdot D^* \cdot C^* + d_2 \cdot D^* \cdot T^* + d_3 \cdot C^*\, T^* \quad (1)$$

where k is a constant, D*, C* and T * are the variables defined in Table 1, and a_i, b_i, c_i, and d_i are coefficients that, along with k, are obtained by stepwise regression.

3. Results and discussion

3.1. Metallosome characterization

In previous studies we worked with supramolecular aggregates formed by metallosurfactants with chains of two and six carbon atoms mixed with SPC. To ensure the preparation of the most stable structures these aggregates were obtained by vortexing. Thus, the formation of spontaneous aggregates minimizes the packing deficiencies caused by the structural differences between the two components. As demonstrated, these differences were able to dramatically change the type of supramolecular aggregate when the metallosurfactant to SPC molar ratio was progressively changed: vesicles, large rods, micelles and bicelles were obtained [25,27]. The subsequent synthesis of TCOL10 aimed to achieve a metallosurfactant with a length similar to that of a biological monolayer; however, surface tension measurements indicated that this molecule could adopt a double-loop conformation in interfaces,[21] a conformation that makes the length of its hydrophobic domain about half of that of phosphatidylcholine. Nonetheless, spontaneous (and large) TCOL10/SPC mixed vesicles were stable. Because small delivery systems are mandatory for biomedical applications, in this work we aimed to further explore the stability of metallosomes when their vesicular size is reduced, that is, when the geometry of the supramolecular aggregates is imposed, for example, by extrusion. Fig. 1 shows the results of DLS analysis of SPC liposomes and TCOL10/SPC 1:3 mol/mol metallosomes obtained after extrusion through specific membrane pores, as described in Section 2.2. As can be observed, there is a strong relationship between the membrane pores and the main peak of

Table 1
Levels of the factors chosen for the cell incubations, their corresponding change of variable (indicated with *) and the increment between two consecutive converted values.

Diameter / nm	D* = Log Diameter	Δ D*	[TCOL10] / μM	C* = Log [TCOL10]	Δ C*	Time / h	T * = Log Time	Δ T *
50	1.7	-	50	1.7	-	1	0	-
100	2.0	0.30	100	2.0	0.30	2	0.3	0.30
200	2.3	0.30	250	2.4	0.40	5	0.7	0.40
400	2.6	0.30	500	2.7	0.30	13	1.11	0.59
800	2.9	0.30	1000	3.0	0.30	26	1.41	0.30

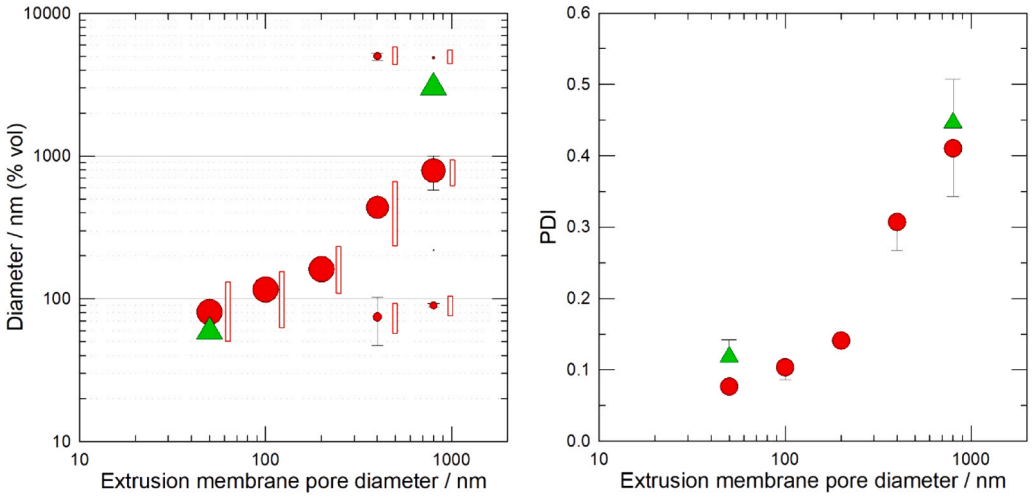

Fig. 1. a) Diameter of peak distributions of SPC liposomes (green triangle) and TCOL10/SPC 1:3 mol:mol metallosomes (red circles) obtained by extrusion through 800, 400, 200, 100 or 50 nm pores. The size of the symbols is proportional to the population of vesicles of each peak. The error bars indicate the standard deviation of the peak diameter, and the vertical red rectangles show the width of the peaks of the metallosomes. b) Polydispersity index of the samples. $n \geq 2$.

all metallosome suspensions. This is especially true for the case of 800, 400, 200 and 100 nm membrane pores (main peaks located at 790, 436, 161 and 116 nm respectively), however, in the case of the smaller pore diameter (50 nm) the metallosomes show a peak at approximately 80 nm, which is 60% higher than that of the pore. This difference was much higher than that observed for SPC liposomes extruded in the same conditions, with a diameter of approximately 60 nm (which makes the metallosomes more than 30% larger than the SPC liposomes). Similar results were found for phosphatidylcholine liposomes by other authors [28], who showed that extensive repeated extrusions through 50 nm pore membranes lead to vesicles of 60–70 nm in diameter. The divergence between the extrusion pore diameter and size of the extruded SPC vesicles occurs when the pore size is close to the geometrical limit of the liposomes, approximately 20 nm. This is due to the membrane tensions and packing defects that such a small size causes (an SPC bilayer is about 4 nm thick, which is 40% of the radius of a liposome of 20 nm in diameter). Thus, the extra size of metallosomes extruded through 50 nm pores has to be a consequence of membrane packing deficiencies originated by TCOL10 that, in turn, limit the minimum size that a stable vesicle of this type can achieve. The results suggest that the minimum diameter of mixed metallosomes should be not far from 50 nm.

The effect of TCOL10 on the membrane is very different in the case of large metallosomes. Note that they are more effectively downsized when extruded through 800 nm pores that SPC liposomes Fig. 1a. At this scale, the membranes are not subjected to the limitation that a small curvature of the radius generates. Then, the difference between the diameter of the 800 nm extruded SPC liposomes and the TCOL10/SPC 1:3 mol/mol metallosomes should be attributed to an increased instability of the metallosomes during size reduction driven by two factors: the aforementioned packing defects and, mainly, the two negative electrical charges of TCOL10, which favor the formation of small vesicles [29,30].

A second point to be considered in size analysis is the polymodality of the 400 and 800 nm extruded metallosomes. This is manifested by the presence of a main vesicle population (similar to the corresponding

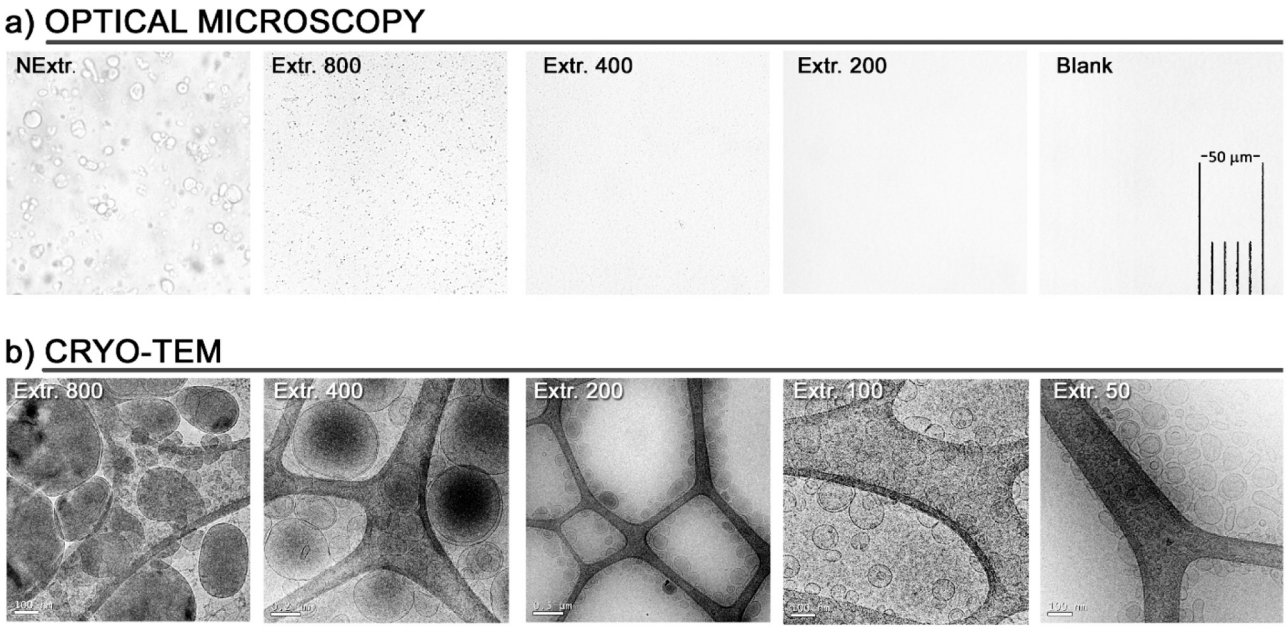

Fig. 2. Optical microscopy (a) and cryo-TEM (b) images of non-extruded (NExtr.) metallosomes, and extruded (Extr.) through 800, 400, 200, 100 and 50 nm pore membranes. In a) the magnification is the same in all the pictures and the scale is shown in the Blank labeled image. In b) the scale bar is in each image.

extrusion pore) along with two minor populations (Fig. 1a) and high PDI values (Fig. 1b). The diameters of the larger metallosome populations were in the upper range of analysis of the DLS device (in the micrometric range); this fact along with the polymodality of the samples generated less precise results. Therefore, the extent of the presence of very large metallosomes was studied by optical microscopy. It should be noted that the study of the existence of micrometric vesicles in suspensions is not marginal because the size of the metallosomes is one of the three factors studied in this work that can modulate cellular uptake. The images (Fig. 2a) show that there was a dramatic change in the size of the vesicles after extrusion through the 800 nm and 400 nm pore membranes. However, the images also show that in these two cases the downsizing process is not fully effective and metallosomes with a diameter larger than the nominal pore of the membranes remain in the suspensions (see the histograms in SupplMat-4). This is not the case for extrusions through pores equal to or smaller than 200 nm; in these cases, the optical fields show no vesicles and are equivalent to those of the blank (slide with aqueous medium). Most studies have characterized the size of extruded vesicles using only the mean diameter obtained by DLS. This procedure is reliable for suspensions free of micrometric aggregates, but the existence of these large vesicles can generate errors in the mean diameter even if they constitute a small part of the population. As shown, a part of the metallosome population of the samples extruded at 800 nm had a diameter of several micrometers. This size is at the limit or even falls outside the device analysis range which means that the vesicles were not detected in the last case. In contrast, the large population of the 400 nm extruded metallosomes is not as large as the previous one and completely falls inside the device range analysis. These two different circumstances make the DLS mean diameter of the 800 nm extruded metallosomes (724 ± 224 nm) smaller than that of the 400 nm extruded vesicles (1764 ± 522 nm), which is clearly an anomalous description of the samples. These previous results allow to have a precise description of the size of the vesicles and indicate that complementary techniques are necessary to fully describe the samples.

To study the morphology of the metallosomes, the samples were analyzed by cryo-electron microscopy (cryo-TEM). The cryo-TEM images (Fig. 2b) showed that in all cases vesicular systems are obtained and most of them contain one or two membranes. The heterogeneity of the samples obtained after 800 and 400 nm pore extrusion can also be observed: small and large (usually dark because they protrude the vitrified film) vesicles were detected. The heterogeneity is even larger if it is taken into account that micrometric vesicles are excluded from the grid during the blotting process because they cannot be retained by the thin aqueous film of the grid holes [31]. The heterogeneity of 800 and 400 nm extruded samples agrees with the results of optical microscopy and DLS analysis and indicates that a very broad vesicle size distribution is obtained during mechanical agitation. Extrusion decreases the heterogeneity being its efficiency higher with the decreasing pore diameter. Thus, DLS, and optical and electron microscopy analyses provide evidence that all extrusions produce vesicular systems that are mainly unilamellar with the main population having a diameter close to that of the membrane pore.

3.2. Metallosome stability

The use of metallosomes as CO-releasing aggregates in biological systems has several advantages over the administration of free CORM molecules in the bulk. One of them is that the aggregates themselves contain a large quantity of active CORMs as they are part of the structure. Furthermore, as a mixed system, they can be decorated and/or functionalized to have long residence times and selective targeting in the same manner as liposomes [32,33]. However, the previous advantages are only valid if the structure of the aggregates is preserved in biological systems, where they undergo high dilution, and if the release of CO can be controlled. The first requirement is not met in the case of pure TCOL10 metallosomes because of the relatively high critical vesicle concentration (CVC) of the metallosurfactant (approximately 0.28 mM) [21]. Therefore, to validate TCOL10/SPC vesicles as a delivery system it was necessary to characterize the behavior of the mixed TCOL10/SPC vesicles under dilution. The study was carried out by DLS comparing the size of the vesicles upon a wide-ranging dilution (up to two orders of magnitude), both at a short time and 26 h after dilution. The systems evaluated were metallosomes extruded through 800, 200 and 50 nm pores, that is, those with a size located at the upper and lower limits of the size range and central value. The results (SupplMat-5) indicate that the three types of metallosomes do not disaggregate upon dilution, that is, TCOL10 is not released and their structure is maintained. Otherwise, a progressive decrease in the vesicle population of a given size should be detected, concomitant with the formation of heterogeneous vesicles formed only by SPC, along with an increase in PDI. This is what is observed, for example, when bicelles composed of phospholipids and short-chain surfactants (with relatively high critical micellar concentration) are diluted: the surfactant escapes from the structure to the bulk (where it exists as monomer) and the remaining phospholipid undergoes a rearrangement to form large and heterogeneous vesicles [34,35]. Consequently, the aforementioned results indicate that TCOL10 metallosomes are stable to dilution more than 10 times below the CVC of the metallosurfactant and that they will maintain their structure at any of the time and concentration conditions of the cell incubation shown in Table 1.

The spontaneous CO release of the metallosomes in the absence of light and its effect on the structural integrity of the metallosomes (extruded through 800, 200 and 50 nm pores) were monitored in parallel using FTIR (inset Fig. 3) and DLS analysis respectively. With regards to CO release, there was no effect of the vesicular size, since the three types of suspensions gave the same results at a given temperature (SupplMat-6). This is why Fig. 3 shows the means obtained at 4 and 37 °C. At 4 °C TCOL10 was stable, for at least 30 days. Nonetheless, this was not the case at 37 °C, and the release of CO was detected after a lag time of approximately four days. Therefore, under dark conditions, TCOL10 (a photoCORM) undergoes spontaneous temperature-

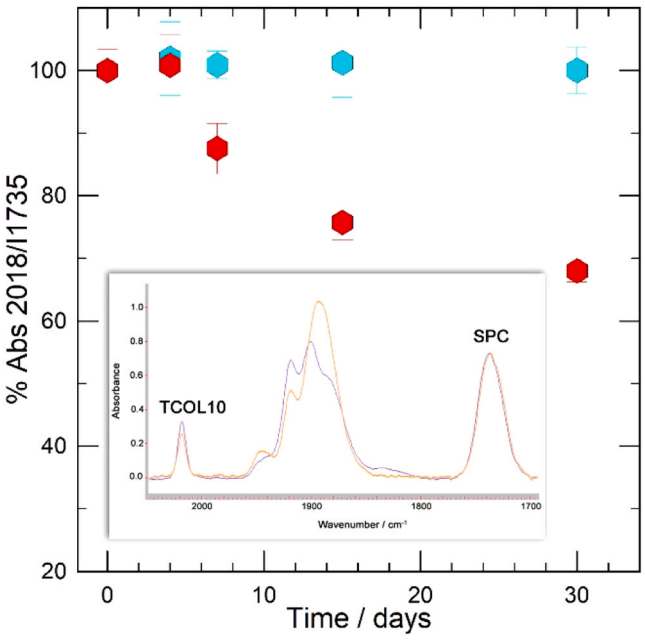

Fig. 3. Chemical stability of TCOL10/SPC 1:3 mM/mM metallosomes upon time, in dark, and at 4 °C (cyan) and 37 °C (red) (mean ± std, n = 2). Inset: normalized infrared spectra of a fresh sample (violet) and after incubation at 37 °C for 30 days (orange). The labels indicate the CO peaks of the metallosurfactant and phosphatidylcholine used to obtain the relative absorbance ratio (% Abs 2018/1735) shown in the main figure.

dependent degradation that, as in the case of other metal carbonyls, should be triggered, for example, by pH and/or oxygen, and lead to ligand substitution/exchange [36]. The lag period indicates that TCOL10 has (at least) two stages of degradation and that temperature regulates the extent of the slow stage, also called the induction phase. This behavior has been observed in hydrogels and colloidal suspensions of polymeric solid particles with or without entrapped drugs, and in most cases their degradation and/or drug release evolution fit sigmoidal models [37–40]. One of the most used is the Prout-Tompkins equation which was developed specifically for the degradation of solids (thermal decomposition of potassium permanganate crystals), but it shows good results in other fields [41,42]. One example is the aforementioned colloidal particles, in which the degradation takes place inside them. The location of the reactions makes solid colloidal systems comparable to the degradation of solids originally considered by the mathematical model. Surprisingly, the model was also successfully applied to characterize events that occur at the particle surface, which also shows a lag period. [43] Thus, it is not unexpected that the evolution of spontaneous CO release from metallosomes (i.e. hollow membrane vesicles) shows characteristics similar to those occurring into solid particles and also on their surface. The observed lag time can be attributed to a protective environment of the hydrophobic region of the mixed membrane on the active part of TCOL10, that is, the Mo-carbonyl complex. The same evolution has been observed by other authors in linoleate liposomes, where lipid peroxidation was studied. [44] Furthermore, the induction phase is not only applied to membrane lipids: several drugs increase their stability (even in photolysis processes) when entrapped into liposomal membranes. In some cases, the protection is mediated by the interaction of the drugs with the phospholipids, as in the case of norfloxacin [45] and cyanocobalamin [46], while in others the isolation from the bulk is the main cause [47,48].

The observed release of CO at 37 °C, compared to that at 4 °C, shows the increase of the rate constant of the chemical degradation of the ligand. The break of the CO-Mo bonds implies changes in the bulky hydrophobic part of TCOL10 (constituted by the Mo complex) which, in turn, can affect membrane packing and vesicle stability. This possibility was evaluated by DLS analysis of the samples in parallel with FTIR analysis. At 4 °C only the peaks of the 800 nm extruded metallosomes show variations (Fig. 4) which are explained by the polymodal character of the size distribution. The other extruded vesicles (which were monodisperse) showed a constant size during the 30 days of the study. With regards to the samples kept at 37 °C, the most remarkable fact was the appearance of micrometric vesicles (~5 μm) after 7 and 30 days of incubation of the 50 and 200 nm extruded metallosomes, respectively. In both cases they were only 10–15% of the total vesicle population and, consequently, the original size was the more abundant even after 30 days of incubation at 37 °C. So, the formation of large vesicles takes place first for the smaller metallosomes, when the CO release is only approximately 10% (Fig. 3), while for the 200 nm extruded vesicles, this value has to reach 30%. This early destabilization of the small metallosomes can be a consequence of TCOL10 structural changes in membranes that are already stressed under normal conditions.

In summary, the data set of the metallosome stability study provides conclusive evidence that the mixed TCOL10/SPC 1:3 mol:mol vesicles meet the stability requirements for their use in biological systems. Their structure is stable upon dilution and in dark, and they show high structural and chemical stability at 37 °C (for a total of 4 days). Altogether, these data validate the system for the cell incubation experimental conditions used in the present study, where TCOL10/SPC was incubated for a maximum of 26 h at 37 °C. Moreover, it has been demonstrated that at 4 °C in the dark metallosomes maintain their chemical and physical properties for a minimum of 30 days.

3.3. Metallosome toxicity

The viability of cells incubated with metallosomes for 26 h is shown in Fig. 5. The results indicate that at 26 h all vesicles had a similar

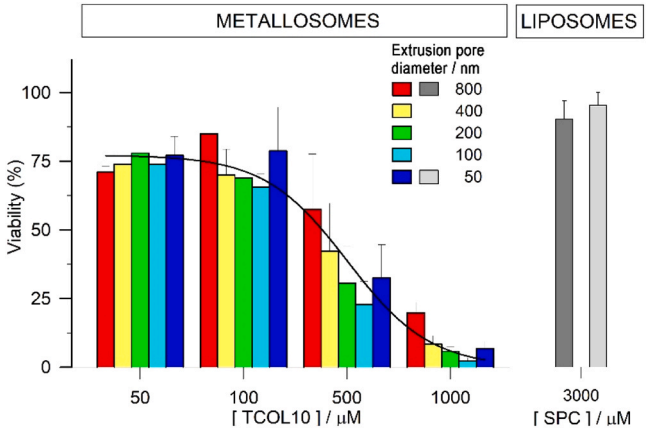

Fig. 5. Cell viability of fibroblasts after 26 h of incubation with TCOL10/SPC 1:3 mol:mol metallosomes (n ≥ 2) and with SPC liposomes (n = 2) at a phospholipid concentration equivalent to that of the maximum of the metallosomes. (Mean ± sem). The curve was obtained using as ansatz a sigmoidal fit of all the metallosome data.

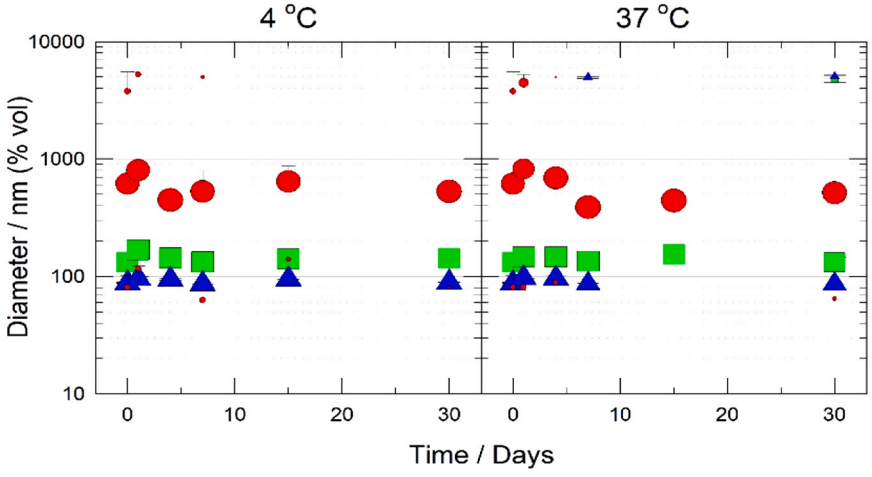

Fig. 4. Peak size distribution of 800 (red circles), 200 (green squares) and 50 nm (blue triangles) extruded TCOL10/SPC 1:3 mM/mM metallosomes upon time during their incubation at 4 °C and 37 °C. The size of the symbols is proportional to the population of vesicles of a given diameter. (Mean ± std, n = 2).

toxicity with a D_{50} between 100 and 500 μM. Previous experiments carried out with mixed systems consisting of SPC and other metallotensioactives of the TCOL10 family (with one or two carbon chains of two or six carbon atoms) showed a higher toxicity when they formed very small structures or were unstable to dilution:[25,27] free metallosurfactants, bicelles, micelles and non-stable vesicular systems that disaggregate upon dilution have a D_{50} between 70 and 170 μM. On the contrary, when these molecules form spontaneous and stable large metallosomes (some micrometers in diameter) they exhibit the same behavior as that of non-toxic SPC liposomes. Thus, it is apparent that at 26 h the extruded TCOL10/SPC metallosomes have a non-existent toxicity in the case of very large stable vesicles and, at the same time, it is smaller than that of the corresponding very small aggregates. In other words, the downsizing of TCOL10/SPC metallosomes increases their toxicity to (and interaction with) the cells but into a lesser extent than the very small metallosurfactant/SPC aggregates. This makes their toxicity halfway between that of small systems and large spontaneous vesicles.

3.4. Cellular uptake of metallosomes

The use of an FTIR microscope with a synchrotron light source allows single-cell spectrum analysis, and owing to the high signal-to-noise ratio, very small quantities of TCOL10 can be detected. In our case, we took advantage of both characteristics to determine the influence of relevant factors such as incubation time, concentration of TCOL10, and vesicular size on the two responses of the system evaluated, that is, the percentage of cells that contained TCOL10 and the strength of the uptake.

The analysis of the CO region of the TCOL10 of 846 spectra (SupplMat-7) indicated that under the experimental conditions located at non-extreme values of the incubation, there was a bimodal cell behavior. Under these conditions some cells showed the CO band of TCOL10 with a similar relative intensity, while in others it was not present at all. This indicates that, under the given experimental conditions, there were two cell populations: one prone to interact with the metallosomes and the other prone not to do so. This is the reason why this behavior was quantified in terms of the percentage of cells that showed the CO band of TCOL10 and characterized by fitting Eq. 1 using the diameter of the main peak of the DLS analysis. The results (SupplMat-8a) indicate that the three independent variables studied influence the response. Fig. 6 shows contour plots calculated from the fitted equation. As expected, the percentage increases with the increase of time and concentration and, more noticeably, it is also affected by the size of the metallosomes. For example, after 26 h of incubation with 1000 μM of TCOL10, the percentage of cells that showed the metallosurfactant in the corresponding spectrum was approximately 60%, 80% and 100% for 80, 200 and 800 nm extruded vesicles respectively (in general, the maximum efficacy is achieved by the 800 nm metallosomes). At short incubation times (1–3 h) it was observed that the TCOL10 concentration had little effect on the percentage. Complementarily, at low TCOL10 concentrations (50–100 μM), the effect of incubation time is also low, but it increasesd with an increase of vesicle size.

Once the percentage was studied, the relative amount of TCOL10 inside the cells was characterized by the CO to amide I intensity ratio. After fitting the coefficients using the experimental vesicle diameter obtained by DLS, Eq. 1 (SupplMat-8b) shows that the three studied parameters also significantly modify the response. As can be seen in Fig. 7a and b, the relationship between the TCOL10 concentration and the ratio is not linear and the slope decreases with an increase in the former. In a general point of view it can be observed that the CO/Amide I ratio increases when vesicle size and concentration increase. With regards to the vesicle size, at long incubation times (Fig. 7a; 26 h) there was a prominent effect at low concentrations: the ratio for the 800 nm metallosomes was 0.15 while it was approximately 0 for the 80 nm vesicles. Note that this difference between both types of vesicles was not as noticeable at high TCOL10 concentrations. In contrast, Fig. 7b shows that the previously exposed effect of vesicular size decreases at short incubation times (5 h).

The influence of incubation time is shown in Fig. 7c and d. At all TCOL10 concentrations and metallosome sizes, the incubation time showed a saturation effect. Regarding the influence of vesicular size, it does not change the ratio at short incubation times, while it is prominent at long times (26 h), particularly if the TCOL10 concentration decreases (Fig. 7d).

Finally, the overall effect of metallosome size can be observed in Fig. 7e and f. In general, the larger the vesicular size (in the studied range) the higher the ratio obtained, which was particularly true at low TCOL10 concentrations and short incubation times.

One implication of the previous results is related to the choice of administration conditions of CO in cell cultures, which can be carried out in two different ways. On the one hand, there is a combination of level factors that causes negligible uptake of metallosomes with a maximum concentration of TCOL10 in the bulk. This situation was achieved with small vesicles (80 nm) and a maximum value of 200 μM TCOL10, and allowed approximately 5 h of incubation with no significant uptake (see Fig. 7f). Since TCOL10 is a photo-CORM, during this interval, the release of CO could be triggered by light, and the gas would reach the cells (it has a high permeability through membranes). On the other hand, the opposite approach is also possible: a set of experimental conditions can be chosen to produce a high vesicular uptake at non-toxic levels. Once the vesicles are internalized, and after removal of the incubation medium, the effect of TCOL10 can be studied both under illumination and in the dark; in both cases, the gas is released directly

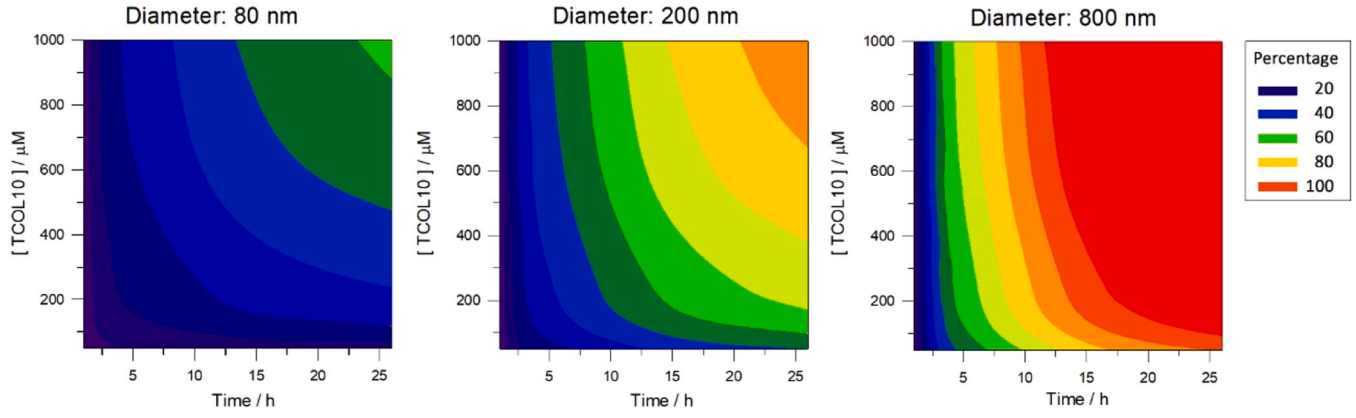

Fig. 6. Contour plots of the percentage of cells that show TCOL10 in their FTIR spectrum as function of incubation time and TCOL10 concentration when incubated with 80, 200 and 800 nm metallosomes. [TCOL10]-axis range: 50–1000 μM; Time-axis range: 1–26 h.

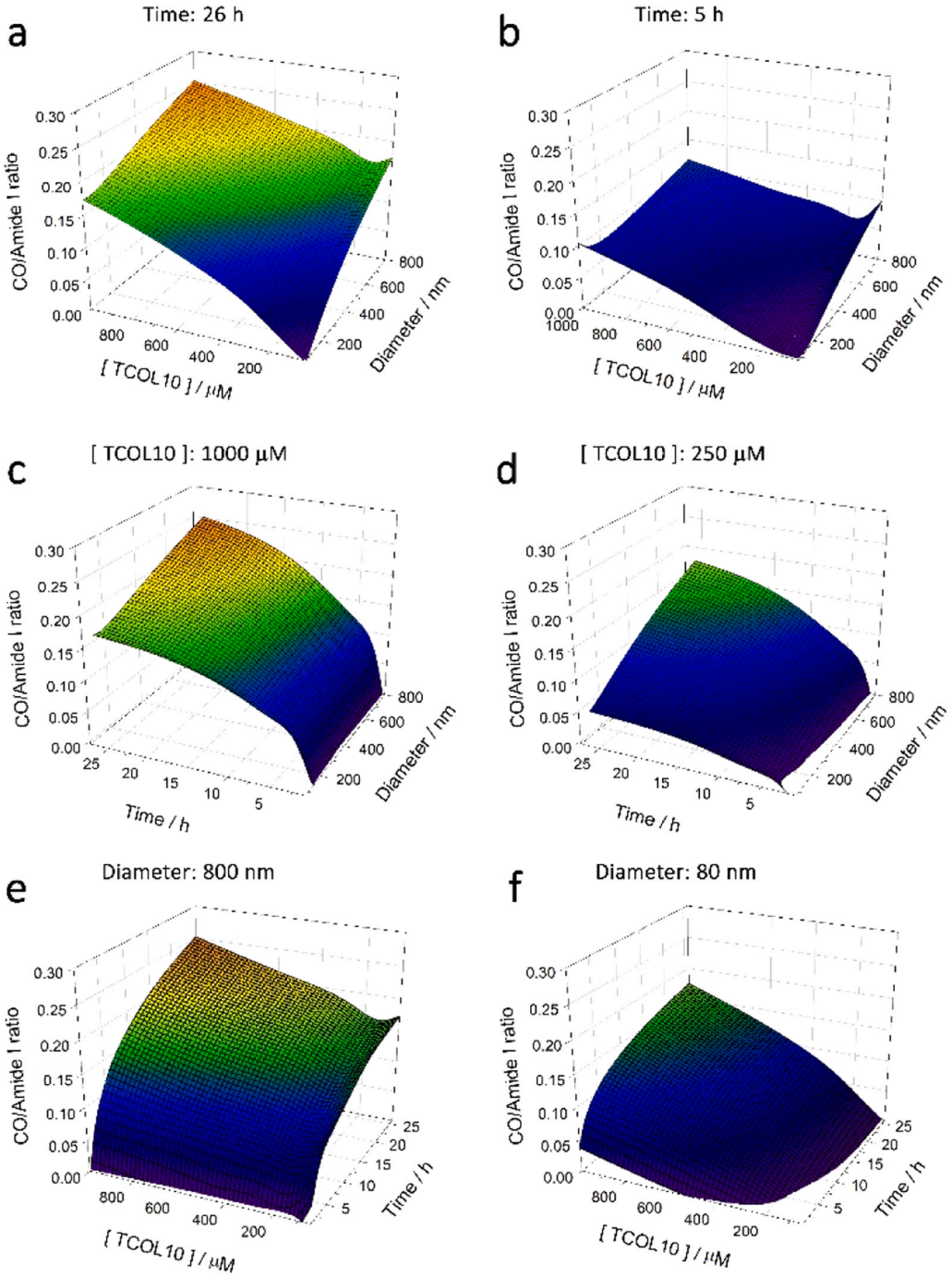

Fig. 7. Surface responses of the CO/Amide I ratio calculated from the model obtained using the cellular FTIR spectra (n = 1215). [TCOL10]-axis range: 50–1000 µM; Diameter-axis range: 80–800 nm; Time-axis range: 1–26 h.

inside the cells. The selection of the method must take into account a main aspect to be studied in next works: the effectiveness of CO achieved by diffusion from the medium or by direct release from internalized vesicles at non-toxic doses in both cases.

Another important issue from the results (both percentage and ratio) is the vesicle-size dependence found: as it has been shown, in the studied range the uptake is favored for large vesicles. This is not surprising because it has also been observed by other authors. In these studies, suspensions were composed of negative liposomes made of saturated phosphatidylcholine/cholesterol/dicetylphosphate (size from 100 nm to 2000 nm) [49] and saturated phospholipid/dicetylphosphate (from 100 nm to 400 nm); [50] neutral and negative unsaturated phospholipids (from unextruded liposomes to 200 nm); [51] and cationic liposomes of unsaturated phosphatidylcholine/dioleoyl-trimethylammonium-propane (from 90 nm to 200 nm). [52] If other types of nanoparticles are considered, such as those with a higher Young's modulus (harder and less deformable than liposomes) and/or a smaller size, a similar behavior is observed. This is true for chitosan particles (150–500 nm) [53] and Ag nanoparticles (5–100 nm). [54] It is also possible to find literature that is not entirely coincident. This is the case of Chuard et al., [55] who studied liposomes from 50 to 400 nm and found a maximum internalization for the 100 nm vesicles. However, in this study, vesicle uptake was mediated by disulfide groups located at the liposomal bilayer, and a specific mechanism of internalization,

different from that of previous cases, should be involved.

From a mechanistic point of view, the dependence of vesicle size on the uptake should be related to the number of collisions per unit of time between vesicles and cells. In this context, it can be assumed that given a certain vesicular membrane composition the driving force for its internalization does not change with vesicular size, since the vesicle surface chemistry and size do not change. In other words, if the type of interaction between vesicles and cells depends solely on their molecular components due to their surface interactions at short distances, thus, the greater the number of collisions between them, the greater the uptake. Column 2 of SupplMat-9 shows the relative number of unilamellar vesicles obtained from those with a diameter of 800 nm. This is the case for the extrusion of unilamellar liposomes and metallosomes in the present work, since they are mainly unillamellar, particularly those of small diameter (Fig. 2b). The values were calculated considering the relationship between the surface of the reference vesicle (which is proportional to the number of molecules) and the total surface of the new ones, that is:

$$4\pi r_{800}^2 \quad = n_i \cdot 4\pi r_i^2 \tag{2}$$

where r_{800} is the radius of the vesicles with a diameter of 800 nm, r_i is the radius of the vesicles with a diameter i, and n_i is the number of vesicles of diameter i. From Eq. 2, the number of vesicles generated is:

$$n_i = \left(\frac{r_{800}}{r_i}\right)^2 \tag{2}$$

As can be seen, at a constant lipid concentration the downsizing process increases the number of vesicles that interact with cells and, therefore, favors their uptake. However, because the vesicular mass is proportional to its surface (not to the volume), during the size reduction the amount of matter that the obtained vesicles contain decreases exactly in an inverse manner to their number (column 3, SupplMat-9). Then, the relative mass contained in a vesicle with diameter i (m_i) to that of an 800 nm diameter (m_{800}) is:

$$m_i \Big/ m_{800} = \left(\frac{r_i}{r_{800}}\right)^2 \tag{4}$$

Consequently, at this point, although the downsizing generates more vesicles, which favors the uptake (via an increase in the number of interactions), the amount of matter internalized should be the same for all vesicular sizes shown in SupplMat-9. However, a decrease in the vesicle size implies faster movement into the bulk according to the Stokes-Einstein law for diffusion in solution, which states that the diffusion coefficient is inversely proportional to the particulate radius (or diameter). Column 4 of SupplMat-9 shows this.

Thus, the mechanistic approach showed that vesicle internalization should increase with decreasing vesicle size, a completely opposite prediction to the results obtained in our uptake experiments and in the works cited above. This means that this approach is incomplete and the existence of other factors that reverse the prediction must be considered.

There are two possible additional factors: those affecting the vesicles and those affecting the cells. With regards to the vesicle factors, a larger diameter implies a larger contact area between vesicles and cells, which should favor uptake. Furthermore, it has been shown that a reduction in vesicle size (from 150 to 20 nm) progressively increases membrane rigidity. [56,57] Some authors have shown by theoretical approaches how vesicle elasticity modulates the internalization process; [58,59] for example, soft vesicles have a high internalization rate after adhesion to the surface has taken place. [60] Relating now to cellular aspects, it is known that cells have different uptake mechanisms. The general term endocytosis includes phenomena such as pinocytosis, phagocytosis, or clathrin and caveolin mediated events, [61,62] which also determine the final destination of internalized particles (i.e. lysosomes, endosomes, cytosol).[50,63] Activation of these processes takes place depending, among other factors, on the size of the vesicles, and globally the overlapping range of action of each one implies that they allow the uptake of particles from about 2 nm to several micrometers (approximately, three internalization pathways ranges are described: till 100 nm, from 100 to 250 nm, and until 5 micrometers). [64] Thus, the different metallosomes studied in the present work could be internalized by different mechanisms due to their size range, which is one order of magnitude (from approximately 80 to 800 nm); that is, their cellular affinity is modulated by their size. Thus, the exposed vesicular factors (soft vesicles, and a large contact area between vesicles and cells) and cellular factors (specific internalization mechanism) can be considered as the main driving force that favor the internalization of large metallosomes found in our study, in opposition to the diffusion effect.

4. Conclusions

The metallosurfactant photoCORM TCOL10 can form mixed vesicles with SPC at a 1:3 molar ratio and the size of the structures can be effectively regulated by extrusion. However, probably due to the double loop conformation of TCOL10 and its impact on the packing of the membranes, the metallosomes show a minimum diameter achievable that is larger than that of pure SPC liposomes. If they metallosome size ranges from 80 to 800 nm in diameter, they are stable to dilution and show chemical and physical stability in dark at 4 °C during, at least, 30 days. However, at 37 °C they showed a spontaneous CO release after a lag time of approximately 4 days and the concomitant formation of a population of large vesicles is also observed. As regards their biological properties, the down-size process makes metallosomes more toxic than very large vesicles with the same composition but less than the very small aggregates formed by pure metallosurfactant. The internalization of metallosomes by cell cultures was effectively characterized as function of incubation time, concentration of TCOL10 and vesicular size: the TCOL10 concentration showed a non-linear relationship with cellular uptake; the incubation time showed a saturation effect; and large particles (800 nm) were more efficiently internalized by the cells than the small ones. The characterization of the system allows two different approaches for CO delivery to the cells: one from the bulk avoiding the cellular uptake and triggering CO release by light; and the second from inside the cells, by means of controlled metallosome internalization. The data indicates that the TCOL10/SPC metallosomes can be considered as a promising CO delivery system for their use in biomedical applications.

Associated content

None.

CRediT authorship contribution statement

Jan Trallero: Investigation, Formal analysis, Writing – review & editing. **Mercedes Camacho:** Investigation, Formal analysis, Writing – review & editing. **Maribel Marín-García:** Investigation, Writing – review & editing. **Elena Álvarez-Marimon:** Investigation, Writing – review & editing. **Núria Benseny-Cases:** Conceptualization, Methodology, Formal analysis, Writing – review & editing. **Ramon Barnadas-Rodríguez:** Conceptualization, Methodology, Formal analysis, Writing – original draft, Supervision.

Declaration of Competing Interest

The authors declare that they have no known competing financial interests or personal relationships that could have appeared to influence the work reported in this paper.

Data Availability

Data will be made available on request.

Acknowledgments

This work was supported by a grant from the Spanish Ministerio de Ciencia e Innovación (PID2021-123682OB-I00). FTIR microscopy experiments were performed at MIRAS beamline at ALBA Synchrotron (reference 2018093029) with the collaboration of ALBA staff. The authors thank Dr. Salvador Bartolome, director of the LLEB-UAB, for providing the use of the FTIR spectrometer. We also want to thank Professor Joan Suades his valuable support from his happy retirement and Dr. Glòria Garcia-Ortega the drawing of the structure of TCOL10.

Author contributions

Jan Trallero and Mercedes Camacho contributed equally to this work.

Appendix A. Supporting information

Supplementary data associated with this article can be found in the online version at doi:10.1016/j.colsurfb.2023.113422.

References

[1] T. Sjöstrand, Endogenous formation of carbon monoxide in man under normal and pathological conditions, Scand. J. Clin. Lab. Investig. 1 (3) (1949) 201–214.
[2] Y. Haili, D. Jiangfeng, Z. Shuang, N. Guangjun, Z. Hui, G. Zhanjun, Z. Yuliang, Emerging delivery strategies of carbon monoxide for therapeutic applications: from CO gas to CO releasing nanomaterials, Small 2019 (2019) 1904382.
[3] R.A. Cazuza, G. Batallé, X. Bai, C.R.A. Leite-Panissi, O. Pol, Effects of treatment with a carbon monoxide donor and an activator of heme oxygenase 1 on the nociceptive, apoptotic and/or oxidative alterations induced by persistent inflammatory pain in the central nervous system of mice, Brain Res. Bull. 188 (2022) 169–178.
[4] X. Yang, W. Lu, C.P. Hopper, B. Ke, B. Wang, Nature's marvels endowed in gaseous molecules I: Carbon monoxide and its physiological and therapeutic roles, Acta Pharm. Sin. B 11 (6) (2021) 434–1445.
[5] C. Steiger, K. Uchiyama, T. Takagi, K. Mizushima, Y. Higashimura, M. Gutmann, C. Hermann, S. Botov, H.-G. Schmalz, Y. Nait, L. Meine, Prevention of colitis by controlled oral drug delivery of carbon monoxide, J. Control. Release 239 (2019) 128–136.
[6] T. Takagi, Y. Naito, Y. Higashimura, K. Uchiyama, T. Okayama, K. Mizushima, K. Katada, K. Kamada, T. Ishikawa, Y. Itoh, Rectal administration of carbon monoxide inhibits the development of intestinal inflammation and promotes intestinal wound healing via the activation of the Rho-kinase pathway in rats, Nitric Oxide 107 (2021) 19–30.
[7] W. Guo, S. Huang, J. An, J. Zhang, F. Dong, J. Dang, J. Zhang, Ultrasound-mediated antitumor therapy via targeted acoustic release carrier of carbon monoxide (TARC-CO), ACS Appl. Mater. Interfaces 14 (45) (2022) 50664–50676.
[8] A. Abuchowski, Sanguinate (PEGylated Carboxyhemoglobin Bovine): mechanism of action and clinical update, *Artif. Organs* 41 (4) (2017) 346–350.
[9] H.I. Choi, A. Zeb, M.S. Kim, I. Rana, N. Khan, O.S. Qureshi, C.W. Lim, J.S. Park, Z. Gao, H.J. Maeng, J.K. Kim, Controlled therapeutic delivery of CO from carbon monoxide-releasing molecules (CORMs), J. Control. Release 350 (2022) 652–667.
[10] X. Yang, W. Lu, M. Wang, C. Tan, B. Wang, "CO in a pill": towards oral delivery of carbon monoxide for therapeutic applications, J. Control Release 338 (2021) 593–609.
[11] F.J. Carmona, C.R. Maldonado, S. Ikemura, C.C. Romão, Z. Huang, H. Xu, X. Zou, S. Kitagawa, S. Furukawa, E. Barea, Coordination modulation method to prepare new metal-organic framework-based CO-releasing materials, ACS Appl. Mater. Interfaces 10 (37) (2018) 31158–31167.
[12] G.Y. Lee, A. Zeb, E.H. Kim, B. Suh, Y.J. Shin, D. Kim, K.W. Kim, Y.H. Choe, H. I. Choi, C.H. Lee, O.S. Qureshi, I.B. Han, S.Y. Chang, O.N. Bae, J.K. Kim, CORM-2-entrapped ultradeformable liposomes ameliorate acute skin inflammation in an ear edema model via effective CO delivery, Acta Pharm. Sin. B 10 (12) (2020) 2362–2373.
[13] C. Steiger, T. Lühmann, L. Meinel, Oral drug delivery of therapeutic gases - carbon monoxide release for gastrointestinal diseases, J. Control. Release 189 (2014) 46–53.
[14] U. Hasegawa, A.J. van der Vlies, E. Simeoni, C. Wandrey, J.A. Hubbell, Carbon monoxide-releasing micelles for immunotherapy, J. Am. Chem. Soc. 132 (51) (2010) 18273–18280.
[15] B. Kaur, G.C. Chaudhary, G. Kaur, Cholesterol-induced physicochemical changes in dodecylamine-based metallosomes: drug entrapping ability and interactions with biological molecules, J. Mater. Chem. B. 7 (2019) 3679–3691.
[16] M.L. Moyá, F.J. Ostos, I. Moreno, D. García, P. Moreno-Gordillo, I. V. Rosado, P. López-Cornejo, J.A. Lebrón, M. López-López, Metallo-liposomes derived from the $[Ru(bpy)_3]^{2+}$ complex as nanocarriers of therapeutic agents, Chemosensors 9 (2021) 90.
[17] J. Wang, A.Z. Wang, P. Lv, W. Tao, G. Liu, Advancing the pharmaceutical potential of bioinorganic hybrid lipid-based assemblies, Adv. Sci. 5 (9) (2018) 1800564.
[18] B. Kaur, N. Kaur, T. Sharma, G. Kaur, G.R. Chaudhary, Metallosurfactant based synthetic liposomes as a substitute for phospholipids to safely store curcumin, Colloids Surf. B Biointerfaces 217 (2022), 112621.
[19] R. Sakla, D.A. Jose, Vesicles functionalized with a CO-releasing molecule for light-induced CO delivery, ACS Appl. Mater. Interfaces 10 (16) (2018) 14214–14220.
[20] P. Garg, B. Kaur, G. Kaur, G.R. Chaudhary, Design and applications of metallo-vesicular structures using inorganic-organic hybrids, Adv. Colloid Interface Sci. 302 (2022), 102621.
[21] E. Parera, F. Comelles, R. Barnadas, J. Suades, Formation of vesicles with an organometallic amphiphile bilayer by supramolecular arrangement of metal carbonyl metallosurfactants, *Chem. Commun.* 47 (15) (2011) 4460–4462.
[22] E. Parera, M. Marín-García, R. Pons, F. Comelles, J. Suades, R. Barnadas-Rodríguez, Supramolecular arrangement of molybdenum carbonyl metallosurfactants with CO-releasing properties, Organometallics 35 (4) (2016) 484–493.
[23] M. Marín-García, N. Benseny-Cases, M. Camacho, R. Barnadas-Rodríguez, Metallosurfactants as carbon monoxide-releasing molecules. *Metallosurfactants: From Fundamentals to Catalytic and Biomedical Applications*, first ed., Wiley-VCH GmbH, 2022, pp. 195–222.
[24] S. Bibi, R. Kaur, M. Henriksen-Lacey, S.E. McNeil, J. Wilkhu, E. Lattmann, D. Christensen, A.R. Mohammed, Y. Perrie, Microscopy imaging of liposomes: from coverslips to environmental SEM, Int J. Pharm. 417 (1–2) (2011) 138–150.
[25] M. Marín-García, N. Benseny-Cases, M. Camacho, Y. Perrie, J. Suades, R. Barnadas-Rodríguez, Metallosomes for biomedical applications by mixing molybdenum carbonyl metallosurfactants and phospholipids, Dalton Trans. 47 (40) (2018) 14293–14303.
[26] S.N. Deming, S.L. Morgan, Experimental Design: A Chemometric Approach, Elsevier, Amsterdam, 1987.
[27] M. Marín-García, N. Benseny-Cases, M. Camacho, J. Suades, R. Barnadas-Rodríguez, Low-toxicity metallosomes for biomedical applications by self-assembly of organometallic metallosurfactants and phospholipids, Chem. Commun. 53 (60) (2017) 8455–8458.
[28] A. Hinna, F. Steiniger, S. Hupfeld, P. Stein, J. Kuntsche, M. Brandl, Filter-extruded liposomes revisited: a study into size distributions and morphologies in relation to lipid-composition and process parameters, J. Liposome Res. 26 (1) (2016) 11–20.
[29] R. Barnadas-Rodríguez, M. Sabés-Xamaní, Liposomes prepared by high-pressure homogenizers, Methods Enzymol. 367 (2003) 28–46.
[30] K. Akashi, H. Miyata, H. Itoh, K.Jr Kinosita, Formation of giant liposomes promoted by divalent cations: critical role of electrostatic repulsion, Biophys. J. 74 (6) (1998) 2973–2982.
[31] M. Almgren, K. Edwards, G. Karlsson, Cryo transmission electron microscopy of liposomes and related structures, Colloid Surf. A 174 (1–2) (2000) 3–21.
[32] H. Abbasi, N. Rahbar, M. Kouchak, P. Khalil Dezfuli, S. Handali, Functionalized liposomes as drug nanocarriers for active targeted cancer therapy: a systematic review, J. Liposome Res. 32 (2) (2022) 195–210.
[33] L. van der Koog, T.B. Gandek, A. Nagelkerke, Liposomes and extracellular vesicles as drug delivery systems: a comparison of composition, pharmacokinetics, and functionalization, Adv. Health Mater. 11 (5) (2022), e2100639.
[34] L. Barbosa-Barros, G. Rodríguez, M. Cócera, L. Rubio, C. López-Iglesias, A. De la Maza, López Olga, Structural versatility of bicellar systems and their possibilities as colloidal carriers, Pharmaceutics 3 (3) (2011) 636–664.
[35] S. Taguchi, B.S. Kang, K. Suga, Y. Okamoto, H.S. Jung, H. Umakoshi, A novel method of vesicle preparation by simple dilution of bicelle solution, Biochem. Eng. J. 162 (2020), 107725.
[36] A.C. Kautz, P.C. Kunz, C. Janiak, CO-releasing molecule (CORM) conjugate systems, Dalton Trans. 45 (45) (2016) 18045–18063.
[37] M.D. Blanco, R.L. Sastre, C. Teijón, R. Olmo, J.M. Teijón, Degradation behaviour of microspheres prepared by spray-drying poly(D,L-lactide) and poly(D,L-lactide-co-glycolide) polymers, Int J. Pharm. 326 (1–2) (2006) 139–147.
[38] M. Vandenhaute, D. Snoeck, E. Vanderleyden, N. De Belie, S. Van Vlierberghe, P. Dubruel, Stability of Pluronic® F127 bismethacrylate hydrogels: reality or utopia? Polym. Degrad. Stab. 146 (2017) 201–211.
[39] S. D'Souza, J.A. Faraj, R. Dorati, P.P. DeLuca, A short term quality control tool for biodegradable microspheres, AAPS PharmSciTech 15 (3) (2014) 530–541.
[40] M. Dunne, I. Corrigan, Z. Ramtoola, Influence of particle size and dissolution conditions on the degradation properties of polylactide-co-glycolide particles, Biomaterials 21 (16) (2000) 1659–1668.
[41] M.E. Brown, The Prout-Tompkins rate equation in solid-state kinetics, *Thermochim. Acta* 300 (1–2) (1997) 93–106.
[42] M.E. Brown, B.D. Glass, Pharmaceutical applications of the Prout-Tompkins rate equation, Int. J. Pharm. 190 (2) (1999) 129–137.
[43] C. Awada, H. Traboulsi, Effect of pH and nanoparticle capping agents on Cr (III) monitoring in water: a kinetic way to control the parameters of ultrasensitive environmental detectors, Micromachines 11 (12) (2020) 1045.
[44] P.A. McPherson, A. Bole, K.A. Cruz, I.S. Young, J. McEneny, A curvilinear approach to the kinetic analysis of linoleate peroxidation in aqueous liposomes by 2,2′azobis (2-amidoinopropane) dihydrochloride, Chem. Phys. Lipids 165 (6) (2012) 682–688.
[45] I. Ahmad, A. Arsalan, S.A. Ali, R. Bano, I. Munir, A. Sabah, Formulation and stabilization of norfloxacin in liposomal preparations, Eur. J. Pharm. Sci. 91 (2016) 208–215.
[46] A. Arsalan, I. Ahmad, S.A. Ali, K. Qadeer, S. Mahmud, F. Humayun, A.E. Beg, The kinetics of photostabilization of cyanocobalamin in liposomal preparations, Int. J. Chem. Kinet. 52 (3) (2020) 207–217.

[47] C.H. Nodari, N.D. De Quadros, R. Chiarentin, F.P. Da Silva, F.D.P. Morisso, M. F. Charão, J.D. Fleck, C.B. De Mattos, A.H. Betti, S.G. Verza, Vortioxetine liposomes as a novel alternative to improve drug stability under stress conditions: toxicity studies and evaluation of antidepressant-like effect, Pharm. Rep. 74 (5) (2022) 969–981.
[48] M.P. Gaetil, P.L. Benfica, L.P. Mendes, M.S. Vieira, J.L. Anjos, A. Alonso, K. R. Rezende, M.C. Valadares, E.M. Lima, Liposomal entrapment of 4-nerolidylcatechol: impact on phospholipid dynamics, drug stability and bioactivity, J. Nanosci. Nanotechnol. 15 (1) (2015) 838–847.
[49] S. Chono, T. Tanino, T. Seki, K. Morimoto, Uptake characteristics of liposomes by rat alveolar macrophages: influence of particle size and surface mannose modification, J. Pharm. Pharmacol. 59 (1) (2007) 75–80.
[50] J.S. Lee, S.Y. Hwang, E.K. Lee, Imaging-based analysis of liposome internalization to macrophage cells: Effects of liposome size and surface modification with PEG moiety, Colloids Surf. B. 136 (2015) 786–790.
[51] C. Kelly, C. Lawlor, C. Burke, J.W. Barlow, J.M. Ramsey, C. Jefferies, S.A. Cryan, High-throughput methods for screening liposome-macrophage cell interaction, J. Liposome Res. 25 (3) (2015) 211–221.
[52] K. Sakai-Kato, K. Yoshida, K.I. Izutsu, Effect of surface charge on the size-dependent cellular internalization of liposomes, Chem. Phys. Lipids 224 (2019), 104726.
[53] C. He, Y. Hu, L. Yin, C. Tang, C. Yin, Effects of particle size and surface charge on cellular uptake and biodistribution of polymeric nanoparticles, Biomaterials 31 (13) (2010) 3657–3666.
[54] M. Wu, H. Guo, L. Liu, Y. Liu, L. Xie, Size-dependent cellular uptake and localization profiles of silver nanoparticles, Int J. Nanomed. 14 (2019) 4247–4259.
[55] N. Chuard, G. Gasparini, D. Moreau, S. Lörcher, C. Palivan, W. Meier, N. Sakai, S. Matile, Strain-promoted thiol-mediated cellular uptake of giant substrates: liposomes and polymersomes, Angew. Chem. Int 56 (11) (2017) 2947–2950.
[56] S. Li, F. Eghiaian, C. Sieben, A. Herrmann, I.A.T. Schaap, Bending and puncturing the influenza lipid envelope, Biophys. J. 100 (3) (2011) 637–645.
[57] N. Delorme, A. Fery, Direct method to study membrane rigidity of small vesicles based on atomic force microscope force spectroscopy, Phys. Rev. E 74 (1) (2006), 030901.
[58] H. Tang, H. Ye, H. Zhang, Y. Zheng, Wrapping of nanoparticles by the cell membrane: the role of interactions between the nanoparticles, Soft Matter 11 (44) (2015) 8674–8683.
[59] X. Yi, H. Gao, Incorporation of soft particles into lipid vesicles: effects of particle size and elasticity, Langmuir 32 (49) (2016) 13252–13260.
[60] X. Yi, H. Gao, Kinetics of receptor-mediated endocytosis of elastic nanoparticles, Nanoscale 9 (1) (2017) 454–463.
[61] S. Behzadi, V. Serpooshan, W. Tao, M.A. Hamaly, M.Y. Alkawareek, E.C. Dreaden, D. Brown, A.M. Alkilany, O.C. Farokhzad, M. Mahmoudi, Cellular uptake of nanoparticles: journey inside the cell, Chem. Soc. Rev. 46 (14) (2017) 4218–4244.
[62] P. Foroozandeh, A.A. Aziz, Insight into cellular uptake and intracellular trafficking of nanoparticles, Nanoscale Res. Lett. 13 (1) (2018), 339.
[63] J. Mosquera, I. García, L.M. Liz-Marzán, Cellular uptake of nanoparticles versus small molecules: a matter of size, Acc. Chem. Res. 51 (9) (2018) 2305–2313.
[64] S. Mazumdar, D. Chitkara, A. Mittal, Exploration and insights into the cellular internalization and intracellular fate of amphiphilic polymeric nanocarriers, Acta Pharm. Sin. B 11 (4) (2021) 903–924.